Molecular Requirements for Transformation of Fallopian Tube Epithelial Cells into Serous Carcinoma[1,2]

Amir A. Jazaeri*, Jennifer L. Bryant*, Hong Park[†], Hui Li[†], Neetu Dahiya*, Mark H. Stoler[†], James Stuart Ferriss*,[3] and Anindya Dutta[‡]

*W. Norman Thornton Division of Gynecologic Oncology, Department of Obstetrics & Gynecology, University of Virginia Health System, Charlottesville, VA, USA; [†]Department of Pathology, University of Virginia Health System, Charlottesville, VA, USA; [‡]Department of Biochemistry and Molecular Genetics, University of Virginia Health System, Charlottesville, VA, USA

Abstract

Although controversial, recent studies suggest that serous ovarian carcinomas may arise from fallopian tube fimbria rather than ovarian surface epithelium. We developed an *in vitro* model for serous carcinogenesis in which primary human fallopian tube epithelial cells (FTECs) were exposed to potentially oncogenic molecular alterations delivered by retroviral vectors. To more closely mirror *in vivo* conditions, transformation of FTECs was driven by the positive selection of growth-promoting alterations rather antibiotic selection. Injection of the transformed FTEC lines in SCID mice resulted in xenografts with histologic and immunohistochemical features indistinguishable from poorly differentiated serous carcinomas. Transcriptional profiling revealed high similarity among the transformed and control FTEC lines and patient-derived serous ovarian carcinoma cells and was used to define a malignancy-related transcriptional signature. Oncogene-treated FTEC lines were serially analyzed using quantitative reverse transcription–polymerase chain reaction and immunoblot analysis to identify oncogenes whose expression was subject to positive selection. The combination of p53 and Rb inactivation (mediated by SV40 T antigen), hTERT expression, and oncogenic C-MYC and HRAS accumulation showed positive selection during transformation. Knockdown of each of these selected components resulted in significant growth inhibition of the transformed cell lines that correlated with p27 accumulation. The combination of SV40 T antigen and hTERT expression resulted in immortalized cells that were nontumorigenic in mice, whereas forced expression of a dominant-negative p53 isoform (p53DD) and hTERT resulted in senescence. Thus, our investigation supports the tubal origin of serous carcinoma and provides a dynamic model for studying early molecular alterations in serous carcinogenesis.

Neoplasia (2011) 13, 899–911

Introduction

Epithelial ovarian cancer is the most lethal female reproductive malignancy, yet our knowledge of its cellular origins and mechanisms of carcinogenesis remains notably incomplete. The study of early events in ovarian carcinogenesis is hampered by the fact that more than 80% of ovarian cancers have already metastasized beyond the ovary at the time of diagnosis. During the last decade, observations in women undergoing risk-reducing (prophylactic) salpingo-oophorectomy due to hereditary breast-ovarian cancer syndrome have led to an increased understanding of early ovarian cancer. Approximately 5% of women undergoing risk-reducing surgery are diagnosed with an occult ovarian cancer (high-grade serous carcinoma in most cases) [1,2]. Most of these early cancers are either located in the fimbrial potion of the fallopian tube or have a coexisting carcinoma *in situ* component in the fimbria [3–5]. Work by Crum, Piek, and others has shown that careful sectioning of fallopian tubes from risk-reducing salpingo-oophorectomy specimens frequently reveals areas of marked cytologic atypia and disorganized growth within the fimbria. These areas have been called carcinoma *in situ* or tubal dysplasia [6,7] and are characterized by positive p53 immunostaining (which correlates with mutations in the *TP53* gene), abnormal proliferation, and DNA damage [8]. Furthermore, approximately a third of morphologically normal fimbria from women *without* hereditary ovarian cancer risk exhibit areas of p53 staining without atypia or abnormal proliferation, referred to as p53 signature or foci [8–10]. Collectively, these observations have led to the hypothesis that most serous carcinomas that are clinically classified as ovarian or peritoneal may in fact arise from the fallopian tube's epithelium. However, given that much of this research has been performed on archival paraffin-embedded tissues, direct testing of this hypothesis has proven difficult. Here, we present direct evidence that, by acquiring oncogene activation and tumor suppressor dysfunction, human fallopian tube epithelial cells (FTECs) can transform into a high-grade carcinoma that closely resembles serous carcinoma. Furthermore, we describe a clinically relevant experimental model that is well suited for investigating the earliest stages of carcinogenesis that are currently undetectable or inaccessible *in vivo*.

Materials and Methods

Primary Cell Cultures of Fallopian Tube Fimbria, Serous Ovarian Carcinomas, and Tumor Xenografts

After institutional review board approval, deidentified fallopian tube fimbrial specimens were obtained from salpingo-oophorectomy specimens performed for benign gynecologic indications by the University of Virginia's tissue procurement facility. Specimens from procedures performed for infectious, inflammatory, or endometriosis-related procedures were excluded. Fimbria were incubated in RPMI supplemented with antibiotics and antimycotics for 3 hours at 4°C, rinsed in sterile phosphate-buffered saline (PBS), and incubated in dispase I solution (0.26 mg/ml) overnight at 4°C. FTECs were harvested from the dispase solution by centrifugation, rinsed with PBS, and plated on collagen I–coated plates (Fisher, Suwanee, GA) in FTEC medium, which consists of Medium 171 (Invitrogen, Carlsbad, CA) supplemented with commercially mixture of cytokines and growth factors (MEGM singlequots; Lonza, Allendale, NJ), and left undisturbed for 3 to 4 days at 37°C in a humidified 5% CO_2 incubator. Cells are propagated on collagen plates for two to three passages and checked for epithelial cell composition using cytokeratin immunofluorescence (see next paragraphs). Before retroviral infection, FTECs are plated onto polystyrene uncoated plates (Corning, Corning, NY) in Dulbecco modified Eagle medium (DMEM) + 10% fetal bovine serum (FBS).

Primary human high-grade ovarian serous carcinoma cell lines were established using a similar protocol. After incubation in RPMI supplemented with antibiotics and antimycotics and PBS wash, tumor explants were minced into 1- to 3-mm pieces before dispase treatment as noted above. Tumor cells were then collected by gently aspirating the dispase digest solution away from any remaining tumor nodules into a fresh tube followed by centrifugation. Cell pellets were then rinsed with PBS and plated in OVT medium, which consists of FTEC medium (see above) + 10% FBS on plastic dishes and left undisturbed for 3 to 4 days at 37°C in a humidified 5% CO_2 incubator. Primary serous ovarian cancer cells are propagated on uncoated polystyrene plates and are checked for epithelial composition by cytokeratin immunofluorescence. After three to four passages, these cells are transitioned to DMEM + 10% FBS for *in vitro* experiments.

Limiting Dilution Cloning

Clones were isolated from FTEC74-OC and FTEC76-OC transformed cell lines by plating the cells at limiting dilution in 96-well plates. Plates were monitored every other day for the presence of single colonies, which were expanded.

Preparation of Retroviral Cocktails

HEK293T human embryonic kidney cell lines were obtained from the American Type Culture Collection (ATCC, Manassas, VA) where cell identity is verified routinely using short tandem repeat analysis, and they are routinely tested for *Mycoplasma* infections. Retroviral vectors, except for the short hairpin constructs, were obtained from Addgene (http://www.addgene.org/pgvec1; presented in Table W1). The short hairpins targeting BRCA1 and luciferase (control) were designed using a Web-based algorithm (http://katahdin.cshl.org/siRNA/RNAi.cgi?type=shRNA) according to previously outlined methods [11] and cloned into pMMP-DEST, a retroviral vector that has been modified to have a Gateway (Invitrogen) cassette in the multicloning site. The final retroviral constructs were confirmed using DNA sequencing. Recombinant retroviral particles were produced by transient transfection of HEK293T cells (ATCC) along with packaging plasmids (pCMV-dR8.91 and pMD2G-VSVG). The medium containing recombinant retrovirus was harvested 36 to 40 hours after transfection. Cellular debris was removed by centrifugation and filtration through a 0.45-µm filter (Millipore, Billerica, MA). Oncogenic and control viral cocktails were formed by mixing equal volumes of the corresponding components (Table W1), aliquoting the mixture, and storing single-use vials at –80°C.

Modeling of FTEC Transformation

Before transduction with OC and CC, the efficiency of a single-FTEC transduction was determined to be relatively constant at approximately 15% using viral particles generated by pBABE-GFP vector. Given this infection efficiency and using the binomial distribution as an approximation, we calculated that 14 retroviral infections would be required to ensure that 90% of the cells were infected at least once. This would also result in 64% being infected at least twice, 35% three times, 15% four times, 5% five times, 1% six times, 0.2% seven times, and 0.03% eight times. Over time, positive selection due to growth advantage leads to predominance of the cells harboring transforming combinations of retrovirally delivered transgenes. FTECs were plated in six-well plates in DMEM + 10% FBS.

For transduction, the normal medium was removed, and FTECs were treated with 1 ml/well of either the oncogenic or the control viral cocktail per well for 14 to 16 hours in the presence of polybrene (4 µg/ml). Cells are washed with PBS, incubated in normal media, and allowed to recover for 32 to 34 hours before the next infection.

Clonogenic Assays

For focus formation assays, cell lines were plated at a density of 1000 cells/well in six-well dishes and allowed to grow in DMEM supplemented with 10% FBS for 7 to 10 days. Resulting colonies were fixed and stained using a mixture of 20% formaldehyde, 80% methanol, and 0.25% crystal violet, and visible colonies were counted. Soft agar colony formation assay was performed by plating a single-cell agar (0.35%) suspension of 5000 cells per well in DMEM + 10% FBS on top of a 1.5% agar-DMEM overlay in a six-well dish. At 14 to 20 days after plating, colonies were stained with 0.005% crystal violet, and the number of colonies was noted.

Xenograft Experiments

Animal experiments were performed at the University of Virginia's Molecular Assessment and Preclinical Studies core facility with the approval of the Institutional Animal Care and Use Committee. Four- to five-week-old Fox Chase SCID mice (strain code 250; Charles River, Wilmington, MA) were housed in pathogen-free laboratory animal housing and allowed to acclimate. Mice were injected intraperitoneally with 2×10^7 FTECs or SKOV3 (ATCC, positive control) cells without Matrigel and observed at least twice a week for tumor formation. Animals were killed once they developed palpable evidence of tumor or at 3 months after injection.

Immunoblot Analysis and Immunofluorescence

Protein was extracted in RIPA or SDS loading buffer. Protein concentration was assayed using a BCA protein assay kit (Pierce, Rockford, IL). About 50 to 100 µg of protein per sample was resolved using Tris-glycine gels (Invitrogen) and transferred onto a nitrocellulose membrane (Amersham, Piscataway, NJ). Immunoblot analysis was performed in the usual fashion using the following primary antibodies: anti-p53, C-MYC, GAPDH, BRCA1, and p27 (Cell Signaling, Danvers, MA); SV40 T Ag, α-tubulin, and p21 (Santa Cruz Biotechnology, Santa Cruz, CA); β-actin (Sigma, St Louis, MO); HRAS (Epitomics, Burlingame, CA); and hTERT (Rockland, Gilbertsville, PA). After primary antibody incubation, membranes were washed and incubated in a horseradish peroxidase–conjugated corresponding secondary antibody for 1 hour. After washes, protein bands were detected using enhanced chemiluminescence (GE Healthcare, Piscataway, NJ). For immunofluorescence, cells were plated on coverslips in six-well plates overnight, fixed in 4% paraformaldehyde in PBS for 10 minutes, and rinsed with several washes of PBS. Coverslips were incubated in blocking solution (PBS with 0.3% Triton X-100 and 5% normal serum) for 1 hour after which the primary antibody, anti–pan cytokeratin (Cell Signaling; 1:200) was added for 1 hour at room temperature. After washes, coverslips were incubated in a fluorescein isothiocyanate–labeled donkey anti-rabbit secondary antibody (Jackson, West Grove, PA), washed, and mounted on slides using mounting medium with 4′,6-diamidino-2-phenylindole (Vector, Burlingame, CA), sealed with nail polish, and viewed immediately. Slides were examined using a fluorescent microscope equipped with an Orca II CCD camera (Hamamatsu, Bridgewater, NJ), and images were acquired using Zeiss software (Dublin, CA).

Immunohistochemistry

Xenograft tissues were harvested at necropsy and fixed in 10% neutral formalin overnight and then transferred to 70% ethanol for 24 to 48 hours. Histologic staining and immunohistochemistry were performed by the pathology core facility and were interpreted by a gynecologic pathologist (M.H.S.). Briefly, after paraffin embedding, 5-µm sections were processed for antigen retrieval by microwave treatment in citrate buffer. The primary antibodies used and corresponding dilutions are presented in Table W2.

Short Interfering RNA Treatment and MTT Assays

siRNA transfections were carried out using RNAimax transfection reagent (Invitrogen) per the manufacturer's protocol. Cells were transfected twice: 24 and 48 hours after plating to achieve maximal knockdown. Oligonucleotides were obtained from Dharmacon (Lafayette, CO), and sequences are provided on request. Cell growth was evaluated 72 hours after the second siRNA transfection using an MTT [3-(4,5-dimethylthiazol-2-yl)-2,5-diphenyltetrazolium bromide] cell growth assay kit (Promega, Madison, WI) according to the manufacturer's instructions.

RNA Extraction and Reverse Transcription–Polymerase Chain Reaction

Total RNA was purified from cultured cells using the RNeasy kit (Qiagen, Santa Clarita, CA) including a DNAse treatment step and quantified with NanoDrop (Thermo Scientific, Portsmouth, NH). Reverse transcription was performed using Transcriptor First Strand Synthesis Kit (Roche, Branchburg, NJ). Quantitative reverse transcription–polymerase chain reaction (RT-PCR) was performed using SYBR Green Mix (Abgene, Rockford, IL) with 61°C annealing temperature on an Applied Biosystems StepOnePlus (Foster City, CA). Internal control glyceraldehyde-3-phosphate dehydrogenase (GAPDH) was detected using Applied Biosystems GAPDH assay.

Microarray Analysis

Five micrograms of total RNA was used to construct biotinylated complementary RNA labeled and hybridized to an Affymetrix microarray chip HG-U133Plus2.0 (Affymetrix, Santa Clara, CA) according to the manufacturer's instructions. The raw data were normalized using the GeneChip–Robust Multiarray Averaging (GC-RMA) algorithm, and analyses were performed using BRB-ArrayTools developed by Dr Richard Simon and the BRB-ArrayTools Development Team.

Results

Use of a Positive Selection Screen to Determine the Molecular Pathways Involved in FTEC Growth and Transformation

We designed our screen based on the current knowledge of molecular alterations in high-grade serous ovarian cancers (reviewed by Bowtell [12] and Kobel et al. [13]), as well as previous research by Kendall et al. [14] on the requirements for transformation of human cells. Table 1 summarizes the molecular pathways targeted along with the corresponding rationale, and the overall approach is depicted in Figure 1. To ensure that our *in vitro* approach was relevant to *in vivo* mechanisms of carcinogenesis, we devised a growth-directed selection approach as opposed to forced (antibiotic) selection. We constructed a cocktail of retroviral vectors to transduce FTEC with potentially oncogenic molecular alterations (Table 1), henceforth referred to as the oncogenic cocktail (OC). As a control for nonspecific

Table 1. Targeted Molecular Alterations in Modeling Serous Carcinogenesis.

Pathway	Rationale	Vector(s)	Reference(s)
TP53	TP53 mutations or dysfunctions are nearly ubiquitous in high-grade serous cancers and also seen tubal carcinoma *in situ*.	pBABE-p53DD pBABE-SV40 LT	[6,39,40]
BRCA1	BRCA1 mutations result in 45% lifetime risk of ovarian cancer. Epigenetic silencing, somatic mutations, and other BRCA1 dysfunctions have been reported in a significant portion of sporadic ovarian cancers.	PMMPmir-BRCA1sh-308 pMMPmir-BRCA1sh-5490	[17,41,42]
C-MYC	Frequently amplified and overexpressed in serous cancers. Inversely correlates with prognosis.	PMSCV-MYC-T58A	[43,46]
HRAS	Whereas Ras mutations are rare in serous ovarian cancers, abnormal activation of downstream growth-stimulatory pathways is a key feature of oncogenesis and required for transformation of human cells.	PBABE-HRAS-G12V	[39,47]
RB	Alterations in the RB-p16-cyclin D1/CDK4-E2F are seen in 50% of ovarian cancers.	pBABE-CCND1$^+$CDK4$^-$R24C pBABE-SV40 LT	[47,48]
hTERT	Telomere maintenance is a key feature of cellular immortalization and transformation and required for prevention cell cycle arrest secondary to senescence or DNA damage response.	pBABE-hTERT	[49,50]
GFP	Used as a negative control	pBABE-GFP	

genetic alterations due to retroviral integration, a control cocktail (CC) was constructed from empty, GFP-expressing, and luciferase-targeting short hairpin RNA retroviral vectors. Two independent primary FTEC lines were transduced in parallel with the OC and CC, and their growth and molecular phenotype were monitored over time. The rationale for the use of an oncogenic cocktail followed by positive selection

Figure 1. A positive selection screen for the identification of transforming molecular alterations in FTEC. Two independent normal primary human FTEC lines were transduced with the oncogenic or control cocktail of retroviral particles creating a heterogeneous cell population harboring various combinations of genetic alterations (depicted as different colored cells). Over time, through natural selection, cells with the most effective growth-promoting genetic alterations are expected to predominate and lead to a transformed phenotype (depicted in orange).

screen is as follows. Single or few oncogene integration events are unable to impart growth advantage or transformation due to barriers present in normal human cells, namely telomere erosion and oncogene-induced senescence [15]. In our model, disruption of these barriers and the resulting transformation would require multiple viral transduction events in the same cell. This occurs only in a small fraction of the primary cells (please also see the Materials and Methods section for additional details). Over time, positive selection due to growth advantage leads to predominance of cells harboring the most advantageous combinations of retrovirally delivered transgenes. Conversely, cells lacking alterations required for growth and bypassing senescence and other barriers to transformation are subject to negative selection and extinction.
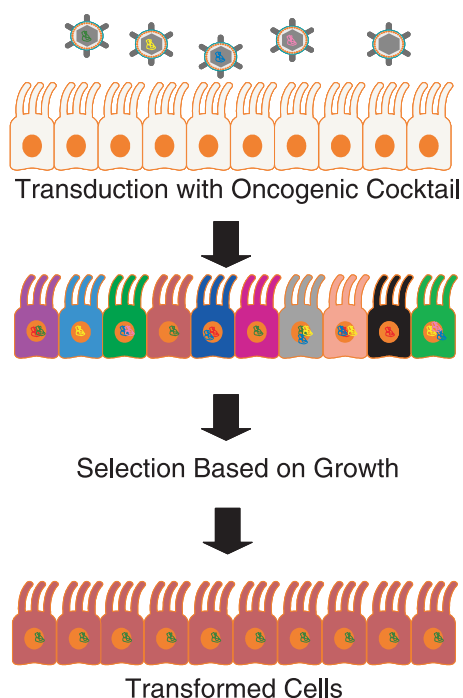
Growth and Transformation of the OC Transduced FTECs

After allowing a 1-month period of recovery after the retroviral infections, growth of the two CC and OC transduced FTEC lines (FTEC74 and FTEC76) was examined using MTT assays (Figure 2A). Both FTEC-OC lines exhibited a small but statistically significant 12% and 17% greater cell numbers at 72 hours compared with the CC-treated counterparts. After three additional months in culture, the differential proliferation became much more apparent with the FTEC74-OC and FTEC76-OC cells exhibiting approximately three times the number of cells in a 72-hour MTT assay (Figure 2A). Given this observation, we performed focus formation assays to look for *in vitro* evidence of transformation of the OC treated cells. Both FTEC74-OC and FTEC76-OC cell lines readily grew and formed foci. In contrast, the FTEC-CC counterparts exhibited little growth and morphologically seemed to be undergoing senescence (Figure 2B). Soft agar colony formation assays were also performed and produced 5 to 15 colonies per well in the OC-treated lines, whereas no colony formation was detected in the FTEC74-CC and FTEC76-CC cell lines (data not shown).

We next investigated the ability of two FTEC-OC cell lines to establish xenografts in SCID mice. By this time, both control cocktail-treated FTEC lines had undergone growth arrest secondary to senescence and, therefore, could not be tested in xenograft studies. Animals were injected intraperitoneally with 2×10^7 FTEC74-OC, FTEC76-OC cells, or SKOV3 cells used as a positive control and monitored
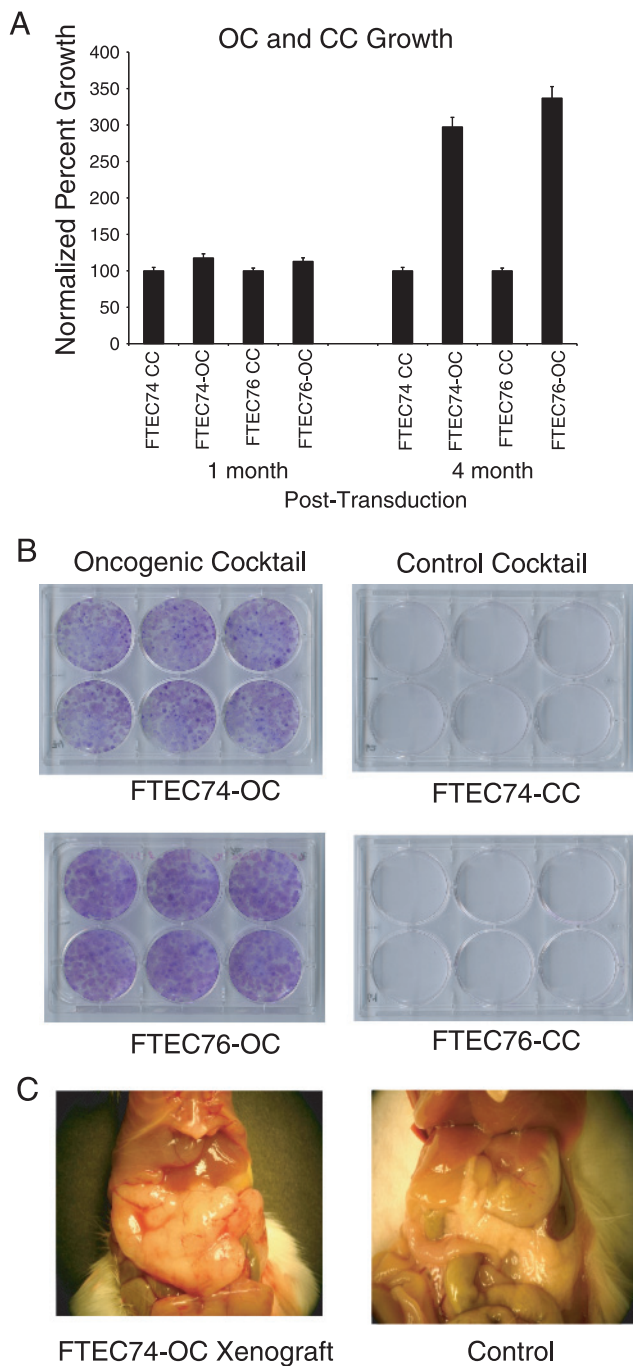
Figure 2. *In vitro* and *in vivo* evidence for FTEC transformation. (A) The oncogenic cocktail–treated FTEC74 and FTEC76 cells exhibited *in vitro* growth advantage that increased with time in culture compared with the control cocktail treated cells as evidenced by 72-hour MTT assays. (B) Focus formation assays performed at approximately 3 months after transduction. (C) Representative example of peritoneal carcinomatosis resulting from intraperitoneal injection of FTEC-OC cells and a normal mouse shown for comparison. Arrows point to tumor encasing the omentum and serosal surfaces of the bowel. This closely resembles the disease distribution seen in patients with advanced stage serous ovarian cancers.

for evidence of tumorigenesis. Both FTEC-OC lines proved capable of establishing xenografts that became detectable at 3 to 4 weeks after injection. The pattern of disease in both FTEC-OC and SKOV3 xenografts was one of peritoneal carcinomatosis including omental

tumor without intraparenchymal organ involvement or lung metastases (Figure 2C).

FTEC-OC Xenografts Recapitulate Poorly Differential Serous Carcinoma

Histologic and immunohistochemical features of the FTEC74-OC– and FTEC76-OC–derived xenografts were very similar; these are presented in Figure 3. The xenografts were composed of poorly differentiated malignant cells with nuclear pleomorphism, prominent nucleoli, frequent mitotic figures, and areas of necrosis (Figure 3, *A* and *B*), consistent with the histologic features of patient-derived poorly differentiated serous carcinoma (Figure 3*C*). The immunohistochemical phenotype of the xenografts also closely resembled that of serous ovarian cancers. The xenografts stained positive for WT1, p53, HE4 (WFDC2), PAX8, and cytokeratin 7 and were negative for cytokeratin 20 (Figure 3, *D-I*).

To investigate the gene expression phenotype of the transformed FTEC lines, we performed transcriptional profiling using the Affymetrix Hgu133plus2 arrays on the two sets of FTEC-OC and FTEC-CC lines as well as three independent primary normal human fallopian tube cell lines and three primary human ovarian serous carcinoma lines (OVTs). Using unsupervised analysis, we determined the overall similarities in gene expression between FTEC, OVT, FTEC-OC, and FTEC-CC groups (Figure 4*A*). Overall, the transcriptional profile of the different cell lines was remarkably similar (with correlation coefficients from pairwise comparisons ranging from 0.7 to >0.9), suggesting that the tissue of origin has a greater influence on transcriptional phenotype than malignant transformation (Figure 4*A*). Next, we generated a list of 123 transcripts that were differentially expressed between the primary normal FTEC and serous cancer cell lines (F test, $P < .005$). Using this gene set, hierarchical clustering segregated the FTEC-OC from FTEC-CC cells quite robustly with a Pearson correlation coefficient of –0.6 between the two groups (Figure 4*B*). To define a transformed/malignant signature, we compared the combined the OVT and transformed FTEC-OC groups to normal FTEC plus FTEC-CC samples (Figure 4*C*). One hundred fifty-eight genes were differentially expressed (F test, $P < .005$) between these groups (Figures 4*C* and W1 and Table W2). In-depth analysis and validation of the differentially expressed genes are the subject of ongoing investigation. However, it is notable that there is little overlap between this list and the lists generated by studies comparing transcriptional profiles of ovarian cancers to normal ovaries or ovarian surface epithelial cells [16–19].

Positive Selection of Oncogenes over Time

To determine which growth-promoting molecular alterations are selected over time and thus contribute to FTEC transformation, we serially examined the expression OC components in both FTEC-OC cells. FTEC74-OC and FTEC76-OC cells were sampled every 3 to 4 weeks after retroviral transduction. In addition, cells from the corresponding xenografts were also examined for the expression of the oncogenic viral cocktail components. The oncogenic cocktail transcripts were assayed using real-time RT-PCR using primers designed to be specific to the retrovirally delivered transgenes with the exception of hTERT and BRCA1 expression where total (endogenous + exogenous) transcript levels were assayed. As depicted in Figure 5, HRAS G12V, hTERT, and SV40 T antigen transgene expression increased over time, whereas C-MYC T58A and CCND1 transcript levels seemed stable over time but were higher in xenografts. In contrast p53DD, a dominant-negative isoform of p53 [20] that was included

in the oncogenic cocktail, showed a transient increased expression in only one of the FTEC lines and no expression in the other cell line. However, this expression was lost over time, consistent with a lack of continuing selection (Figure 5). A GFP-expressing vector was included in both the OC and the CC. Its expression was barely detectable early after viral transduction and was then lost in both FTEC-OC cells. Interestingly, the CC-treated FTECs showed a moderate selection for GFP expression over time, which may have resulted from exposure to a much higher dose of GFP vector in the CC mix and/or secondary retroviral integration effects.

To further evaluate oncogene selection, temporal expression of OC proteins was evaluated using Western blot analysis; this is presented in Figure 6. Although minor variations between the two OC-treated FTEC lines were observed, overall, both demonstrated accumulation of C-MYC, HRAS, hTERT, and SV40 T antigen proteins during *in vitro* transformation and in the corresponding xenografts (Figure 6A). In contrast, GFP levels significantly declined, and cyclin D1 levels remained constant over time. Interestingly, in this model, the selection of SV40 T seemed to negate any selection advantage for the other components of the oncogenic cocktail targeting the p53 and Rb pathways (i.e., dominant-negative p53 (p53DD), and CCND1$^+$CDK4$^-$R24C). In correlation with SV40 T antigen selection, p53 protein also showed increased expression over time but without any detectable p21 expression (Figure 6A). We suspect that the observed p53 accumulation resulted from SV40 T antigen–induced interruption of normal p53 function. Normally, p53 induction leads to a rapid activation of a negative feedback loop involving MDM2,

resulting in rapid degradation of p53 [21]. In contrast, p53 inactivation (due to somatic mutations in ovarian cancers or SV40 T expression in our model) results in paradoxical p53 accumulation. We tested this hypothesis by knocking down SV40 T in FTEC74-OC and FTEC76-OC cells. Suppression of SV40 T rescued p53 dysfunction as evidenced by a decrease in the abnormal accumulation of p53 and increased p21 (Figure 6B).

Previous studies have reported abnormal p27 (Kip1, CDKN1B) expression in 33% to 72% of epithelial ovarian cancers as well as in areas of p53 immunostaining in the fallopian tube's epithelium that have been suggested as possible precursors to serous carcinoma [9,22]. We therefore investigated p27 expression in our model system. Notably, p27 expression was present at the earliest time point analyzed in both FTEC-OC cells lines and persisted in their corresponding xenografts (Figure 6A). This suggests that increased p27 levels may be an early response to oncogenic stress, which, in turn, could lead to further selection of oncogenes that antagonize p27, such as C-MYC [23].

Finally, given that the OC contained two short hairpin constructs targeting BRCA1, the observed temporal increase in BRCA1 at the transcript and protein levels in both FTEC-OC lines was unexpected (Figures 5 and 6A). This may indicate selection against BRCA1 short hairpin RNA–transduced cells. However, we also noted that, in mouse models of SV40 large and small T antigen–induced carcinogenesis, tumors in several tissue types exhibited a common transcriptional signature that included increased BRCA1 expression compared with the corresponding normal tissues [24]. This led us to hypothesize
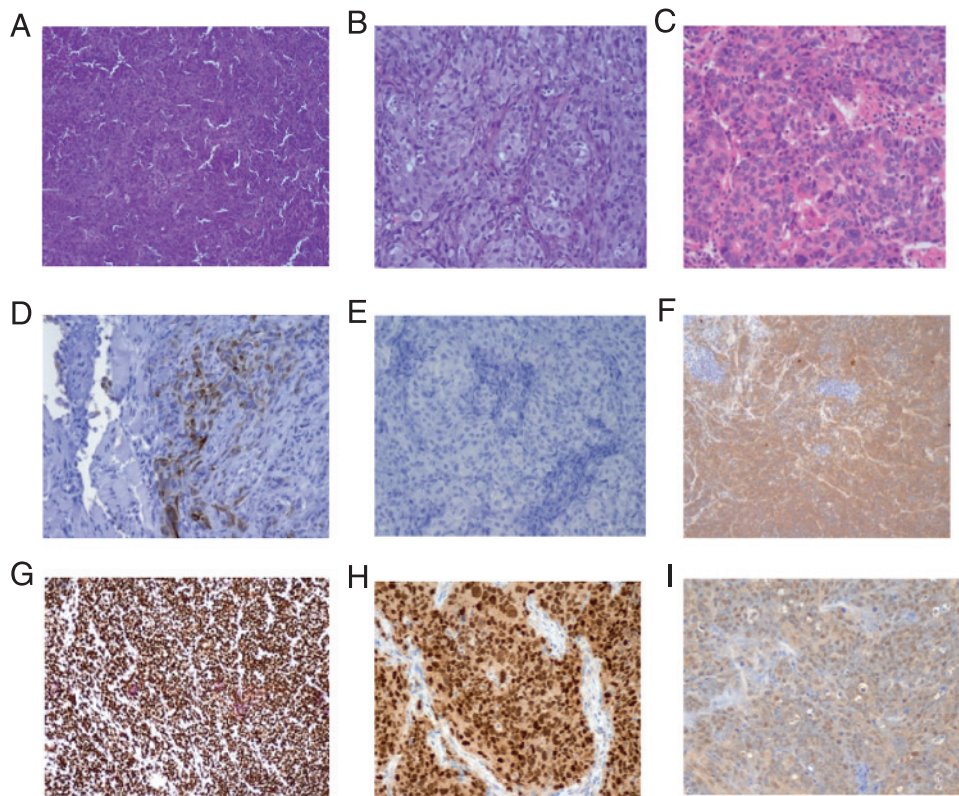
Figure 3. Histologic and immunohistochemical features of FTEC-OC derived xenografts. Representative low (A, ×20) and high (B, ×200) magnification of hematoxylin and eosin–stained sections of FTEC76-OC–derived xenografts and a poorly differentiated patient serous ovarian carcinoma (C, ×200). Immunohistochemical characterization of the xenografts using antibodies targeting cytokeratin 7 (D), cytokeratin 20 (E), HE4 (also known as WFDC2, F), p53 (G), PAX8 (H), and WT1 (I).

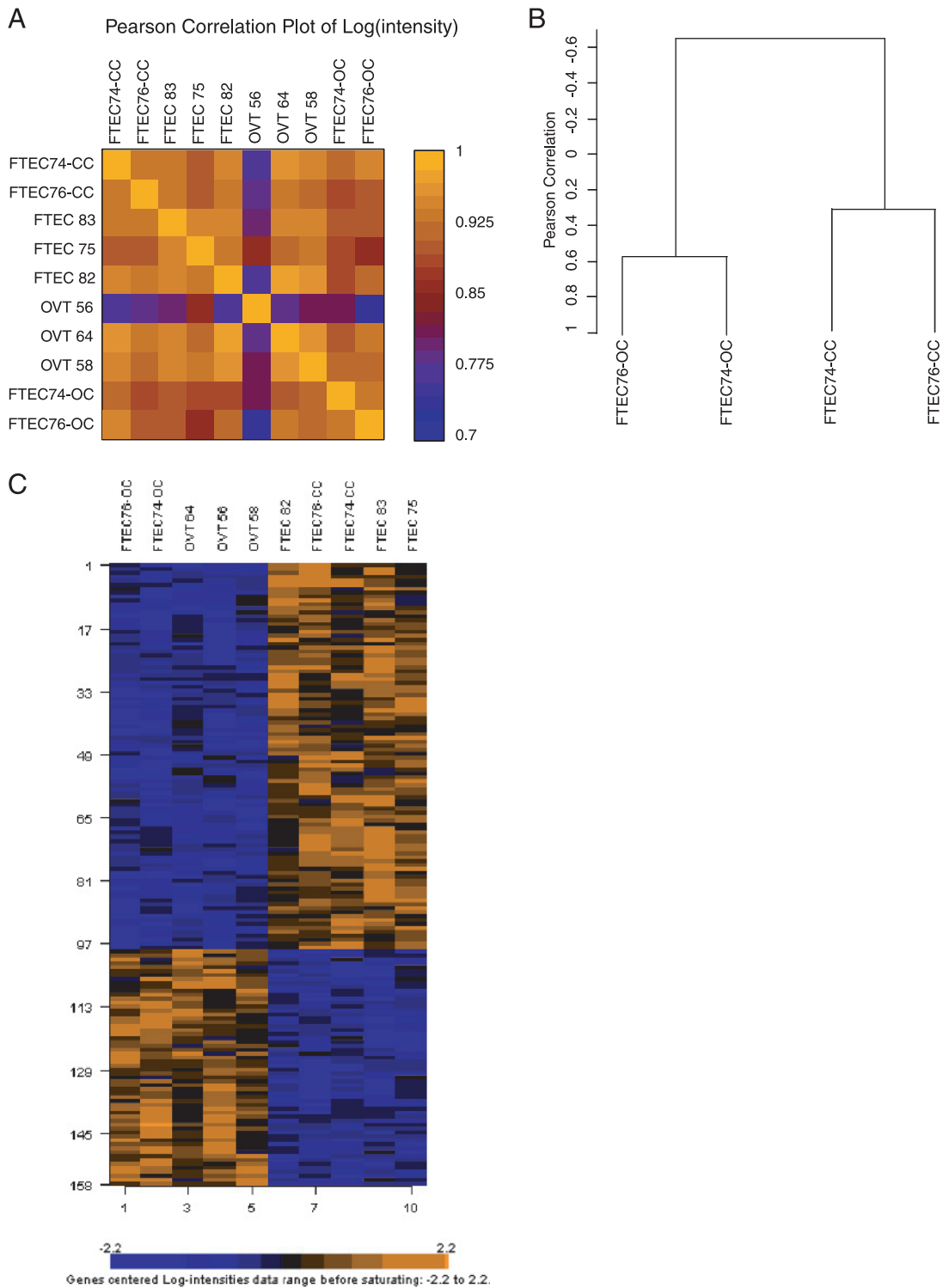**Figure 4.** Transcriptional profiling of FTEC and primary serous ovarian cancer cells. (A) Unsupervised pairwise Pearson correlation coefficients between untreated FTEC, FTEC-OC, FTEC-CC, and primary ovary cancer (OVT) cell lines. (B) The set of 123 transcripts that differentiate untreated FTEC and OVT cells also segregate FTEC-OC and FTEC-CC cells into anticorrelated clusters. (C) A malignancy-related gene list was derived by comparing the profiles of OVT and transformed FTEC-OC cells to those of normal FTEC and the FTEC-CC cells (see Supplementary Data for the identities and expression levels of the 158 transcripts).

that the temporal increase in BRCA1 expression in FTEC-OC cells may be related to SV40 T antigen selection. To test this hypothesis, we depleted SV40 T in FTEC74-OC and FTEC76-OC cells using siRNA. Knockdown of SV40 T led to the loss of BRCA1 protein

and (Figure 6C) transcript (data not shown). These data, together with the previously mentioned study by Deeb et al., suggest that BRCA1 is positively regulated by SV40 T. The mechanisms for this regulation await further investigation.
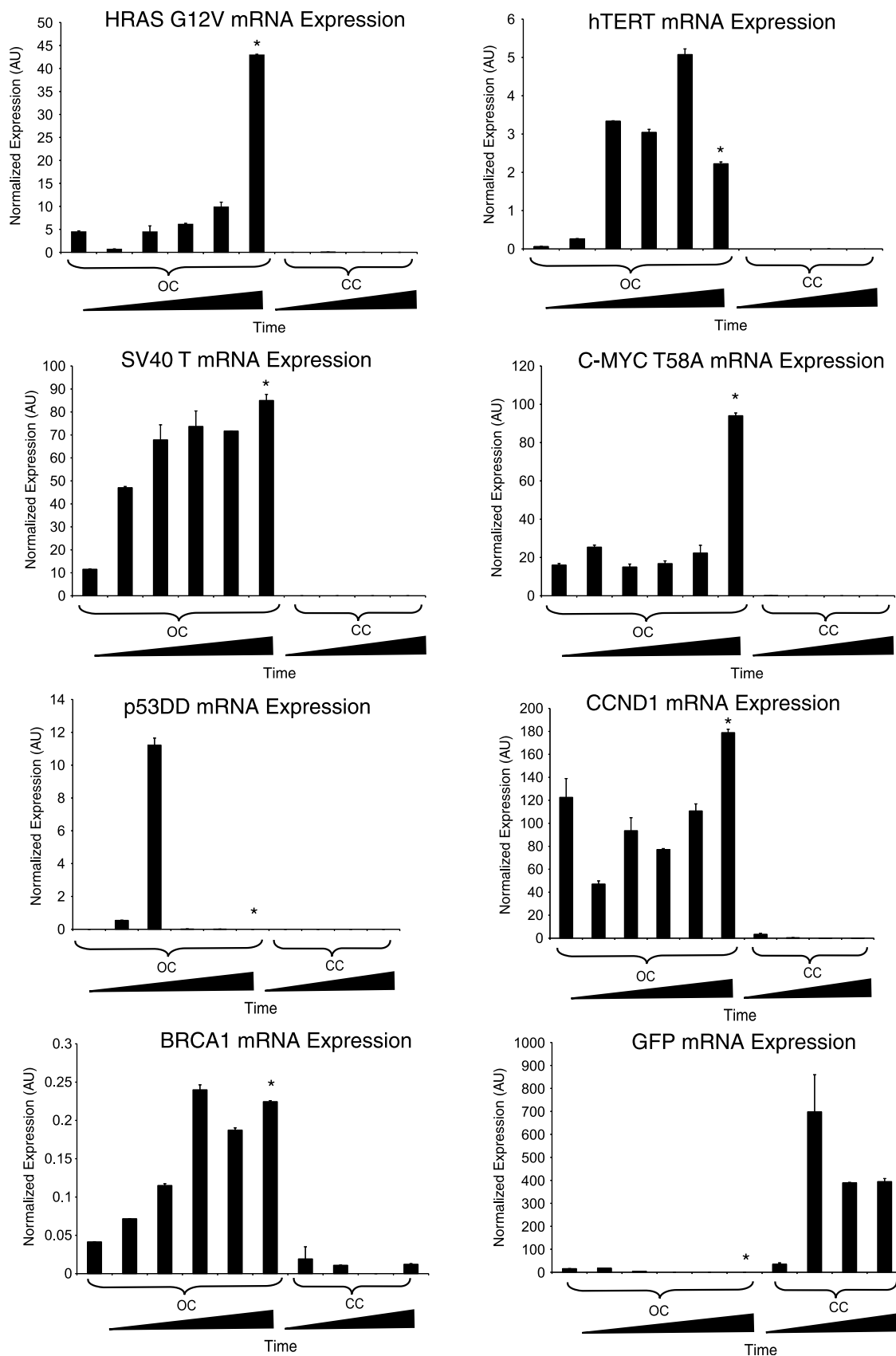
Figure 5. Serial analysis of the components of oncogenic cocktail expression. Quantitative RT-PCR was used to evaluate the expression of various OC and CC components at successive time points (approximately every 3 weeks) during *in vitro* culture of FTEC76 cells, as well as in cell lines established from the FTEC76-OC–derived xenograft (demarcated by an asterisk). Primers used were specific to specific to the retrovirally transduced transgenes with the exception of hTERT and BRCA1 expression where total transcript levels were assayed. Similar patterns of expression were observed in the FTEC74 cell line (data not shown).

Figure 6. Expression of OC-related proteins during FTEC-OC transformation. (A) FTEC-76 and 74 OC cells were sampled at early and late time points after transduction and subjected to Western blot analysis along with cell lines established from their respective xenografts (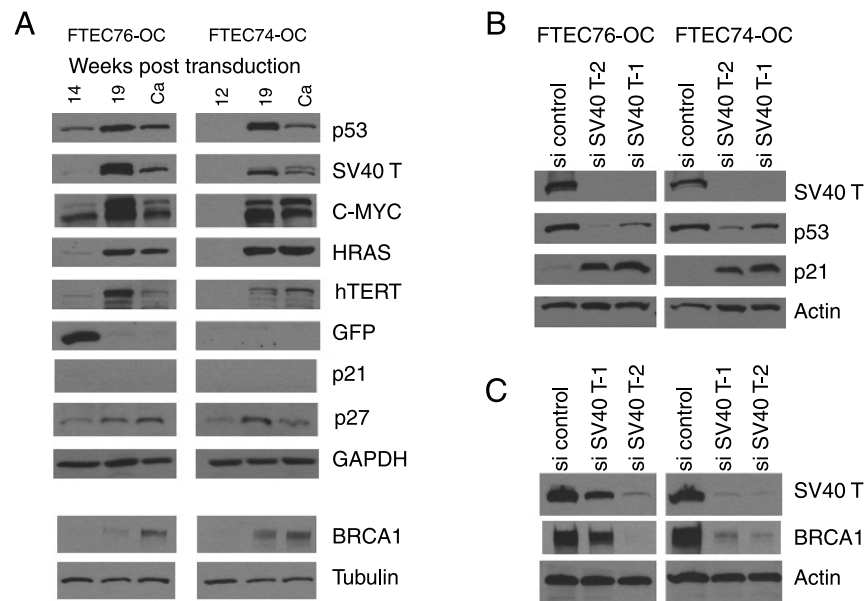Ca). (B) Knockdown of SV40 T antigen rescues inactive p53 accumulation and leads to the induction of p21. (C) Knockdown of SV40 T results in decreased BRCA1 expression.

Clonal Analysis Reveals Coexpression of Oncogenes

On the basis of our experimental design, we hypothesized that transformation of FTEC necessitated the transduction of multiple oncogenic events in the same cell. Whereas the above serial oncogene expression data were consistent with such a model, they did not preclude the possibility that the transformed cell lines were composed of discrete subpopulations expressing some but not all of the oncogenes selected in the parental cell lines. To address this possibility, we used limiting dilution to obtain five single-cell–derived sublines from each of the FTEC-OC–transformed parental lines. The expression levels of SV40 T, C-MYC T58A, and HRAS G12V were assayed in the parental and clonal cell lines using real-time RT-PCR (Figure W2). As expected, the clonal cell lines exhibited varying levels of each oncogene compared with the parental line. More importantly, this analysis confirmed that each of the 10 clones had become transduced by all three selected oncogenes. These results further validate our experimental model by demonstrating that the transformed cells generated harbor the full complement of oncogenic alterations identified through serial expression analysis.

Knockdown of the Selected Oncogenes Inhibits the Growth of Transformed FTEC Lines

To test whether continued expression of OC components was important for the growth of transformed FTEC-OC cells, we performed siRNA experiments aimed at suppressing the expression of the OC components that showed positive selection in these cell lines (Figure 7). Proliferation of both cell lines was significantly decreased after knockdown of HRAS, C-MYC, hTERT, and SV40 T. Interestingly, there was no additive effect associated with knocking down both C-MYC and HRAS, suggesting that these oncogenes may have a cooperative effect on the growth of the transformed FTECs. Next, we considered if this growth inhibition could be mediated through cyclin-dependent kinase inhibitors. Our earlier results had shown that,

in our model, SV40 T selection correlates closely with p53 dysfunction and p21 suppression (Figure 6, A and B). We hypothesized that because of its known antagonistic relationship with C-MYC, p27 (CDKN1B) may also be involved. Knockdown of the selected oncogenes using siRNA resulted in increased p27 expression (Figure 7C), suggesting that suppression of p27 may be important for the continued growth of the transformed FTECs.

Fewer Molecular Alterations Are Not Sufficient for the Transformation of FTEC

The previously mentioned experiments revealed that activation of MYC, RAS, and hTERT in addition to interference with p53 and Rb tumor suppressor pathways (through SV40 T expression) was required for FTEC transformation. To investigate the possibility that expression of fewer molecular alterations may also be sufficient for transformation, we studied a number of oncogenic combinations (summarized in Table 2). We began by testing the effects of forced expression of hTERT and SV40 T oncoprotein. After transduction and antibiotic selection, the resulting FTEC-SV40 T + hTERT cells grew well *in vitro* and were able to avoid senescence, which was uniformly observed in the control FTECs after 8 to 12 weeks in culture. However, none of four SCID mice injected with FTEC-SV40 T + hTERT cells formed xenografts. Interestingly, transduction of these FTEC-SV40 T + hTERT cells with a vector expressing both C-MYC T58A and HRAS G12V did result in transformation. To test whether expression of both HRAS G12V and C-MYC T58A oncogenes was necessary for FTEC transformation, we investigated two FTEC lines that were treated with an OC lacking HRAS G12V. These cells grew readily *in vitro*; however, even 20 weeks after intraperitoneal injection, none of four SCID mice formed tumors, whereas FTECs treated with OC, which that included HRAS G12V, formed xenografts in both animals with a latency of approximately 4 weeks.
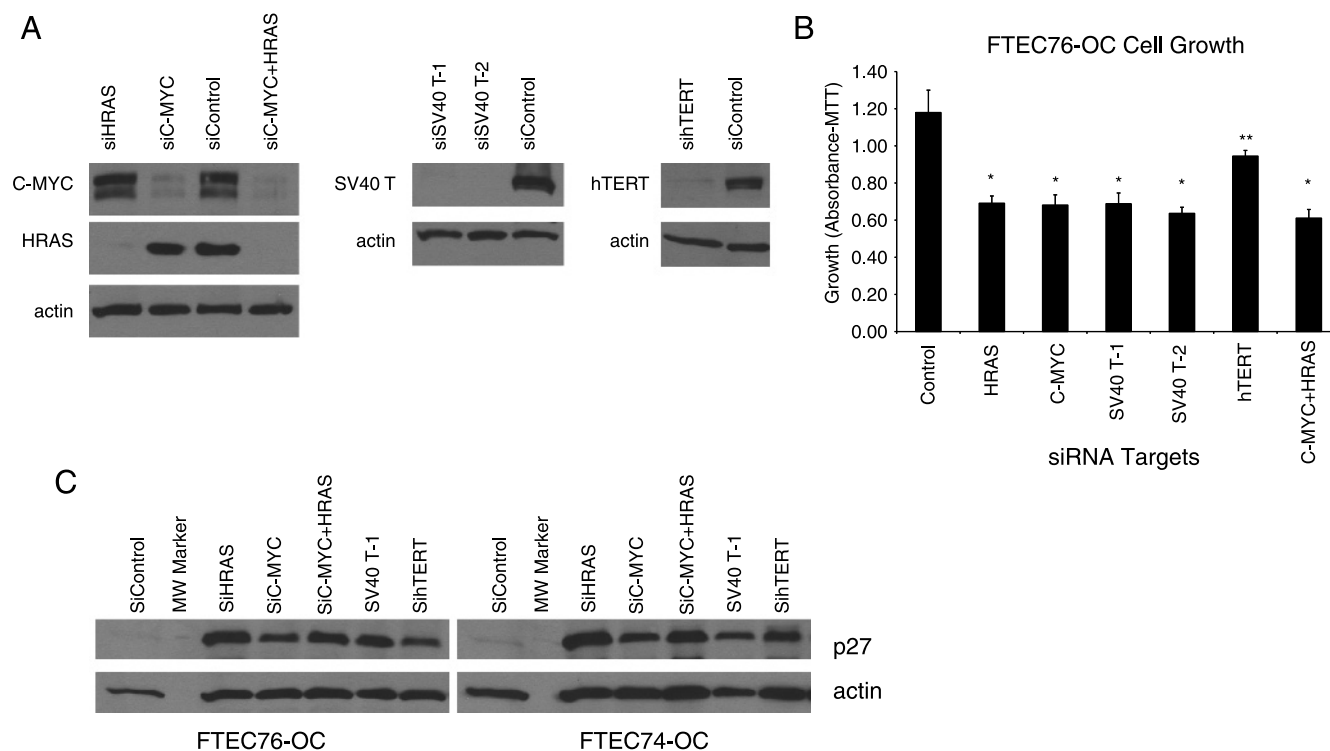
Figure 7. Effects of oncogene knockdown in FTEC-OC cells. (A) siRNA target protein levels. (B) Growth of control and siRNA-treated FTEC76-OC (72 hours). *$P < .0001$. **$P < .005$. Error bars represent SD. (C) Induction of p27 after siRNA treatment.

Given the ubiquitous and early involvement of p53 mutations in serous ovarian carcinomas and their proposed histologic precursors, we investigated the effects of combined forced telomerase activity (through hTERT expression) and p53 dysfunction (through expression of dominant-negative p53DD). Six independent FTEC lines were transduced and selected to force the expression of hTERT and p53DD. All underwent growth arrest morphologic changes consistent with senescence regardless of whether hTERT was overexpressed first followed by p53DD or vice versa. This occurred despite evidence of p53DD expression, wild-type p53 dysfunction, and telomerase activation as demonstrated by telomere repeat amplification protocol assay (data not shown). Thus, the combination of p53 dysfunction and telomerase activation is not sufficient for the continued proliferation of human FTEC.

Finally, after a period of sustained growth, we observed a slow down in FTEC74-OC cells. Serial assay of the cell line using RT-PCR revealed a decline of hTERT expression, whereas FTEC76-OC line showed retained hTERT and proliferation (data not shown).

To test whether decreased hTERT expression was the cause of growth slowdown, FTEC74-OC cells were treated with either an empty retrovirus or pBabe-hTERT-neo followed by neomycin selection. FTEC74-OC cells with forced hTERT expression regained rapid proliferation, whereas the control vector–transduced cells underwent growth arrest and senescence.

Taken together, these observations further support the findings of our oncogenic selection model, stating that inhibition of both p53 and Rb pathways as well as activation of MYC, RAS, and telomerase is required for the transformation of human FTEC.

Discussion

The uncertainty surrounding the tissue of origin of serous carcinoma, the main histologic subtype of epithelial ovarian cancer, remains a significant obstacle confronting a better understanding of the pathophysiology of this disease. Our research provides direct evidence supporting the fallopian tube origin of serous carcinoma and provides

Table 2. Summary of Molecular Alterations and Associated Phenotypes.

Genetic Alteration	Growth	Focus Formation	Senescence	Xenograft (Intraperitoneal Injection)
FTEC-CC	+	N	Y	ND
FTEC-OC	+++	+++	N	Y
FTEC-OC with lost hTERT expression	+	ND	Y	ND
FTEC-OC with forced hTERT expression	+++	+++	N	Y
FTEC-OC without HRAS-G12V expression	+++	+++	N	N (0/4 mice)
SV40 T + hTERT	+	+	N	N (0/4 mice)
SV40 T + hTERT + HRAS G12V + C-MYC T58A	++	++	N	Y
HTERT + p53DD	+/−	ND	N	ND

N indicates not observed; ND, not done due to growth arrest/senescence; Y, observed.

insights into the prerequisite molecular events required for the transformation of human FTEC. We found that the minimal alterations sufficient for transformation of human FTECs are interference with p53 and Rb tumor suppressor pathways (as accomplished by SV40 T oncoprotein), telomerase expression, and activation of Myc and Ras pathways. These findings are consistent with observations of Kendall et al. who showed that forced activation of MYC, RAS, and hTERT in addition to interference with p53 and Rb tumor suppressor functions were necessary and sufficient to transform human cells of epithelial and mesenchymal origin [13].

While this article was in preparation, Karst et al. [25] published their work on immortalization and subsequent transformation of primary human fallopian tube epithelial cells. Although the methodologies differ, overall, the findings of these two studies are very consistent, and the phenotype of the transformed FTECs in both studies are quite similar and phenocopy that of patient-derived serous carcinomas commonly classified as ovarian or peritoneal cancer. Karst et al. immortalized FTECs first by using forced expression of SV40 T, SV40 t (small t antigen), and hTERT. They found that addition of C-MYC or oncogenic HRAS resulted in the transformation of xenografts in immunocompromised mice, albeit, with different potencies [25]. In our study, we used growth rather than antibiotic selection and found that FTECs harboring SV40 T, hTERT, HRAS G12V, and C-MYC T58A expression are selected over time in culture and achieve transformation. The fact that our results showed selection of both C-MYC T58A and HRAS G12V may be explained by a greater growth advantage of cells harboring both mutations. The clonal analysis of our transformed cells revealed that all 10 clones from the two independent transformed FTEC lines had undergone transduction with both HRAS G12V and C-MYC T58A vectors (as well as SV40 T). Furthermore, we observed that FTECs treated with an OC containing C-MYC T58A but not oncogenic HRAS were unable to form tumors in SCID mice. These results strongly suggest that the coexpression of these oncogenes in the same FTEC is required for transformation. Additional evidence supporting the independent contribution of the C-MYC and HRAS oncoproteins to FTEC transformation and cell growth is gained from our knockdown experiments. If discrete populations of transformed cells relied on either C-MYC or HRAS expression, knocking down both oncogenes would be expected to have an additive inhibitory effect on proliferation. However, our experimental evidence reveals no such additive effect (Figure 7, A and B). Finally, the inclusion of SV40 t in Karst's model may have compensated for the requirement of both oncogenes. For example, SV40 t has been shown to stabilize C-MYC by inhibiting serine-threonine protein phosphatase A (PP2A)–mediated dephosphorylation of serine 62 thereby blocking C-MYC degradation [26]. Thus, immortalized FT cells that were transformed in the presence of oncogenic HRAS alone in the model of Karst et al. may also have indirect activation of the C-MYC pathway through SV40 t expression.

Our investigation suggests that p27 protein accumulation may be indirectly involved in FTEC transformation. Because C-MYC opposes p27-induced arrest [23,27], increased p27 levels may act as a selection factor for genetic alterations that result in C-MYC activation. Furthermore, we observed that knockdown of C-MYC, hTERT, HRAS, and SV40 T was associated with decreased cell proliferation that correlated with increased p27 levels, pointing to the potential importance of this cyclin-dependent kinase inhibitor in acting as a barrier to growth and transformation. Interestingly, Norquist et al. [9] observed a decreased p27 expression in tubal p53 foci (areas

of presumed premalignant changed in tubal epithelium) exclusively in BRCA1 mutation carriers. This raises the intriguing possibility that one potential contribution of BRCA1 dysfunction may be related to the ineffective p27 response in at-risk tubal epithelium.

This investigation is the first to define a serous carcinoma–related gene expression profile using untransformed fallopian tube epithelial cells as the reference. It is notable that the list of differentially expressed genes in our study is distinct compared with previously published ovarian cancer transcriptional profiling studies. This is not surprising given that the list of differentially expressed genes is largely dependent on the choice of the normal tissue used for comparison [18]. We believe that FTECs represent a more relevant normal comparison and thus may lead to identification of ovarian cancer biomarkers that are more closely related to the pathophysiology of this disease. In fact, two of the most promising recently developed markers for serous ovarian cancer, HE4 (WFDC2) and PAX8, were both initially identified in several expression profiling studies in which ovarian cancers were compared with normal ovarian tissue, ovarian surface cells, or a composite reference RNA consisting of mixture of various human tissue RNAs [19,28]. However, PAX8 and HE4 are also expressed in normal fallopian tube epithelium [29,30] and, as such, may represent markers of tissue of origin rather than ovarian carcinoma's malignant phenotype *per se*. In this regard, PAX8 has been proposed as a specific marker for secretory FTEC [31,32]. Given that most serous carcinomas are immunohistochemically positive for PAX8 [29,32,33], it has been proposed that secretory FTECs are the cells of origin of serous carcinomas [34]. Our finding of uniform PAX8 positivity in the transformed FTEC74-OC and FTEC76-OC cell lines would be consistent with such a hypothesis. However, we believe that more rigorous testing is needed before PAX8 expression can be considered a definitive proof that secretory FTECs are the exclusive precursor cell type for serous carcinomas. PAX8 is expressed in a number of normal and malignant gynecologic tissues including ovarian inclusion cysts [32]. Furthermore, our primary FTEC cultures were composed of a mixture of secretory and ciliated cells. Although it is possible that secretory cells were preferentially transformed in our model, PAX8 positivity in transformed cells could also be a secondary marker of dedifferentiation or transformation. Interestingly, Yamanouchi et al. [35] have shown that, in the mouse, mesenchymal cells can determine the secretory *versus* the ciliated differentiation of oviductal epithelial cells. This raises the intriguing possibility that stromal cell interactions may play a role in serous carcinogenesis by influencing the phenotype or susceptibility of FTECs. In support of this hypothesis, interactions between cancer-associated and senescent fibroblasts and ovarian cancer epithelial cells have been recently described [36,37].

Finally, the currently proposed model for serous carcinogenesis suggests that p53 mutations or other dysfunction as evidenced by p53 immunostaining may be the earliest precursor to serous carcinomas [5]. In our investigation, induced p53 dysfunction (using a dominant-negative isoform) in combination with telomerase activation consistently led to FTEC growth arrest (presumably due to senescence). This suggests that other early molecular alterations are necessary to enable FTECs with acquired p53 dysfunction to bypass senescence. Alternatively, our model of p53 dysfunction using a dominant-negative isoform may not be able to completely recapitulate clinically observed p53 mutations, which may possess additional gain-of-function properties [38].

In summary, we believe that *in vitro* models of serous carcinogenesis, such as the one described here, have the potential to provide a

better understanding of early events in serous carcinogenesis that are currently clinically undetectable.

Acknowledgments

References

[1] Lamb JD, Garcia RL, Goff BA, Paley PJ, and Swisher EM (2006). Predictors of occult neoplasia in women undergoing risk-reducing salpingo-oophorectomy. *Am J Obstet Gynecol* **194**, 1702–1709.

[2] Laki F, Kirova YM, This P, Plancher C, Asselain B, Sastre X, Stoppa-Lyonnet D, Salmon R, and for the IC-BOCRSG IC-BOCRSG: Institut Curie — Breast Ovary Cancer Risk Study Group (2007). Prophylactic salpingo-oophorectomy in a series of 89 women carrying a BRCA1 or a BRCA2 mutation. *Cancer* **109**, 1784–1790.

[3] Callahan MJ, Crum CP, Medeiros F, Kindelberger DW, Elvin JA, Garber JE, Feltmate CM, Berkowitz RS, and Muto MG (2007). Primary fallopian tube malignancies in BRCA-positive women undergoing surgery for ovarian cancer risk reduction. *J Clin Oncol* **25**, 3985–3990.

[4] Crum CP, Drapkin R, Kindelberger D, Medeiros F, Miron A, and Lee Y (2007). Lessons from BRCA: the tubal fimbria emerges as an origin for pelvic serous cancer. *Clin Med Res* **5**, 35–44.

[5] Folkins AK, Jarboe EA, Roh MH, and Crum CP (2009). Precursors to pelvic serous carcinoma and their clinical implications. *Gynecol Oncol* **113**, 391–396.

[6] Lee Y, Miron A, Drapkin R, Nucci MR, Medeiros F, Saleemuddin A, Garber J, Birch C, Mou H, Gordon RW, et al. (2007). A candidate precursor to serous carcinoma that originates in the distal fallopian tube. *J Pathol* **211**, 26–35.

[7] Piek JM, Verheijen RH, Kenemans P, Massuger LF, Bulten H, and van Diest PJ (2003). BRCA1/2–related ovarian cancers are of tubal origin: a hypothesis. *Gynecol Oncol* **90**, 491.

[8] Folkins AK, Jarboe EA, Saleemuddin A, Lee Y, Callahan MJ, Drapkin R, Garber JE, Muto MG, Tworoger S, and Crum CP (2008). A candidate precursor to pelvic serous cancer (p53 signature) and its prevalence in ovaries and fallopian tubes from women with BRCA mutations. *Gynecol Oncol* **109**, 168–173.

[9] Norquist BM, Garcia RL, Allison KH, Jokinen CH, Kernochan LE, Pizzi CC, Barrow BJ, Goff BA, and Swisher EM (2010). The molecular pathogenesis of hereditary ovarian carcinoma: alterations in the tubal epithelium of women with BRCA1 and BRCA2 mutations. *Cancer* **116**, 5261–5271.

[10] Shaw PA, Rouzbahman M, Pizer ES, Pintilie M, and Begley H (2009). Candidate serous cancer precursors in fallopian tube epithelium of BRCA1/2 mutation carriers. *Mod Pathol* **22**, 1133–1138.

[11] Paddison PJ, Cleary M, Silva JM, Chang K, Sheth N, Sachidanandam R, and Hannon GJ (2004). Cloning of short hairpin RNAs for gene knockdown in mammalian cells. *Nat Methods* **1**, 163–167.

[12] Bowtell DD (2010). The genesis and evolution of high-grade serous ovarian cancer. *Nat Rev Cancer* **10**, 803–808.

[13] Kobel M, Huntsman D, and Gilks CB (2008). Critical molecular abnormalities in high-grade serous carcinoma of the ovary. *Expert Rev Mol Med* **10**, e22.

[14] Kendall SD, Linardic CM, Adam SJ, and Counter CM (2005). A network of genetic events sufficient to convert normal human cells to a tumorigenic state. *Cancer Res* **65**, 9824–9828.

[15] Bartek J, Bartkova J, and Lukas J (2007). DNA damage signalling guards against activated oncogenes and tumour progression. *Oncogene* **26**, 7773–7779.

[16] Gomez-Raposo C, Mendiola M, Barriuso J, Hardisson D, and Redondo A (2010). Molecular characterization of ovarian cancer by gene-expression profiling. *Gynecol Oncol* **118**, 88–92.

[17] Jazaeri AA, Yee CJ, Sotiriou C, Brantley KR, Boyd J, and Liu ET (2002). Gene expression profiles of BRCA1-linked, BRCA2-linked, and sporadic ovarian cancers. *J Natl Cancer Inst* **94**, 990–1000.

[18] Zorn KK, Jazaeri AA, Awtrey CS, Gardner GJ, Mok SC, Boyd J, and Birrer MJ (2003). Choice of normal ovarian control influences determination of differentially expressed genes in ovarian cancer expression profiling studies. *Clin Cancer Res* **9**, 4811–4818.

[19] Welsh JB, Zarrinkar PP, Sapinoso LM, Kern SG, Behling CA, Monk BJ, Lockhart DJ, Burger RA, and Hampton GM (2001). Analysis of gene expres-sion profiles in normal and neoplastic ovarian tissue samples identifies candidate molecular markers of epithelial ovarian cancer. *Proc Natl Acad Sci USA* **98**, 1176–1181.

[20] Shaulian E, Zauberman A, Ginsberg D, and Oren M (1992). Identification of a minimal transforming domain of p53: negative dominance through abrogation of sequence-specific DNA binding. *Mol Cell Biol* **12**, 5581–5592.

[21] Bond GL, Hu W, and Levine AJ (2005). MDM2 is a central node in the p53 pathway: 12 years and counting. *Curr Cancer Drug Targets* **5**, 3–8.

[22] Gadducci A, Cosio S, Tana R, and Genazzani AR (2009). Serum and tissue biomarkers as predictive and prognostic variables in epithelial ovarian cancer. *Crit Rev Oncol Hematol* **69**, 12–27.

[23] Vlach J, Hennecke S, Alevizopoulos K, Conti D, and Amati B (1996). Growth arrest by the cyclin-dependent kinase inhibitor p27^{Kip1} is abrogated by c-myc. *EMBO J* **15**, 6595–6604.

[24] Deeb KK, Michalowska AM, Yoon CY, Krummey SM, Hoenerhoff MJ, Kavanaugh C, Li MC, Demayo FJ, Linnoila I, Deng CX, et al. (2007). Iden-tification of an integrated SV40 T/t-antigen cancer signature in aggressive hu-man breast, prostate, and lung carcinomas with poor prognosis. *Cancer Res* **67**, 8065–8080.

[25] Karst AM, Levanon K, and Drapkin R (2011). Modeling high-grade serous ovarian carcinogenesis from the fallopian tube. *Proc Natl Acad Sci USA* **108**, 7547–7552.

[26] Yeh E, Cunningham M, Arnold H, Chasse D, Monteith T, Ivaldi G, Hahn WC, Stukenberg PT, Shenolikar S, Uchida T, et al. (2004). A signalling path-way controlling *c-myc* degradation that impacts oncogenic transformation of hu-man cells. *Nat Cell Biol* **6**, 308–318.

[27] Prathapam T, Aleshin A, Guan Y, Gray JW, and Martin GS (2010). p27^{Kip1} mediates addiction of ovarian cancer cells to MYCC (c-MYC) and their depen-dence on MYC paralogs. *J Biol Chem* **285**, 32529–32538.

[28] Schaner ME, Ross DT, Ciaravino G, Sorlie T, Troyanskaya O, Diehn M, Wang YC, Duran GE, Sikic TL, Caldeira S, et al. (2003). Gene expression patterns in ovarian carcinomas. *Mol Biol Cell* **14**, 4376–4386.

[29] Ozcan A, Shen SS, Hamilton C, Anjana K, Coffey D, Krishnan B, and Truong LD (2011). PAX 8 expression in non-neoplastic tissues, primary tumors, and metastatic tumors: a comprehensive immunohistochemical study. *Mod Pathol* **24**, 751–764.

[30] Galgano MT, Hampton GM, and Frierson HF Jr (2006). Comprehensive anal-ysis of HE4 expression in normal and malignant human tissues. *Mod Pathol* **19**, 847–853.

[31] Levanon K, Ng V, Piao HY, Zhang Y, Chang MC, Roh MH, Kindelberger DW, Hirsch MS, Crum CP, Marto JA, et al. (2010). Primary *ex vivo* cultures of human fallopian tube epithelium as a model for serous ovarian carcinogenesis. *Oncogene* **29**, 1103–1113.

[32] Bowen NJ, Logani S, Dickerson EB, Kapa LB, Akhtar M, Benigno BB, and McDonald JF (2007). Emerging roles for PAX8 in ovarian cancer and endosal-pingeal development. *Gynecol Oncol* **104**, 331–337.

[33] Laury AR, Hornick JL, Perets R, Krane JF, Corson J, Drapkin R, and Hirsch MS (2010). PAX8 reliably distinguishes ovarian serous tumors from malignant mesothelioma. *Am J Surg Pathol* **34**, 627–635.

[34] Levanon K, Crum C, and Drapkin R (2008). New insights into the pathogenesis of serous ovarian cancer and its clinical impact. *J Clin Oncol* **26**, 5284–5293.

[35] Yamanouchi H, Umezu T, and Tomooka Y (2010). Reconstruction of oviduct and demonstration of epithelial fate determination in mice. *Biol Reprod* **82**, 528–533.

[36] Schauer IG, Sood AK, Mok S, and Liu J (2011). Cancer-associated fibroblasts and their putative role in potentiating the initiation and development of epithe-lial ovarian cancer. *Neoplasia* **13**, 393–405.

[37] Lawrenson K, Grun B, Benjamin E, Jacobs IJ, Dafou D, and Gayther SA (2010). Senescent fibroblasts promote neoplastic transformation of partially transformed ovarian epithelial cells in a three-dimensional model of early stage ovarian cancer. *Neoplasia* **12**, 317–325.

[38] Brosh R and Rotter V (2009). When mutants gain new powers: news from the mutant p53 field. *Nat Rev Cancer* **9**, 701–713.

[39] Hahn WC, Dessain SK, Brooks MW, King JE, Elenbaas B, Sabatini DM, DeCaprio JA, and Weinberg RA (2002). Enumeration of the simian virus 40 early region elements necessary for human cell transformation. *Mol Cell Biol* **22**, 2111–2123.

[40] Ahmed AA, Etemadmoghadam D, Temple J, Lynch AG, Riad M, Sharma R, Stewart C, Fereday S, Caldas C, Defazio A, et al. (2010). Driver mutations in TP53 are ubiquitous in high grade serous carcinoma of the ovary. *J Pathol* **221**, 49–56.

[41] King MC, Marks JH, Mandell JB, and New York Breast Cancer Study Group (2003). Breast and ovarian cancer risks due to inherited mutations in BRCA1 and BRCA2. *Science* **302**, 643–646.

[42] Press JZ, De Luca A, Boyd N, Young S, Troussard A, Ridge Y, Kaurah P, Kalloger SE, Blood KA, Smith M, et al. (2008). Ovarian carcinomas with genetic and epigenetic BRCA1 loss have distinct molecular abnormalities. *BMC Cancer* **8**, 17.

[43] Hemann MT, Bric A, Teruya-Feldstein J, Herbst A, Nilsson JA, Cordon-Cardo C, Cleveland JL, Tansey WP, and Lowe SW (2005). Evasion of the p53 tumour surveillance network by tumour-derived MYC mutants. *Nature* **436**, 807–811.

[44] Skirnisdottir IA, Sorbe B, Lindborg K, and Seidal T (2011). Prognostic impact of p53, p27, and C-MYC on clinicopathological features and outcome in early-stage (FIGO I-II) epithelial ovarian cancer. *Int J Gynecol Cancer* **21**, 236–244.

[45] Goode EL, Chenevix-Trench G, Song H, Ramus SJ, Notaridou M, Lawrenson K, Widschwendter M, Vierkant RA, Larson MC, Kjaer SK, et al. (2010). A genome-wide association study identifies susceptibility loci for ovarian cancer at 2q31 and 8q24. *Nat Genet* **42**, 874–879.

[46] Staebler A, Karberg B, Behm J, Kuhlmann P, Neubert U, Schmidt H, Korsching E, Burger H, Lelle R, Kiesel L, et al. (2006). Chromosomal losses of regions on 5q and lack of high-level amplifications at 8q24 are associated with favorable prognosis for ovarian serous carcinoma. *Genes Chromosomes Cancer* **45**, 905–917.

[47] Kendall SD, Adam SJ, and Counter CM (2006). Genetically engineered human cancer models utilizing mammalian transgene expression. *Cell Cycle* **5**, 1074–1079.

[48] Corney DC, Flesken-Nikitin A, Choi J, and Nikitin AY (2008). Role of p53 and Rb in ovarian cancer. *Adv Exp Med Biol* **622**, 99–117.

[49] Counter CM, Hahn WC, Wei W, Caddle SD, Beijersbergen RL, Lansdorp PM, Sedivy JM, and Weinberg RA (1998). Dissociation among *in vitro* telomerase activity, telomere maintenance, and cellular immortalization. *Proc Natl Acad Sci USA* **95**, 14723–14728.

[50] Shay JW and Wright WE (2010). Telomeres and telomerase in normal and cancer stem cells. *FEBS Lett* **584**, 3819–3825.

Table W1. Viral and Control Cocktail Components.

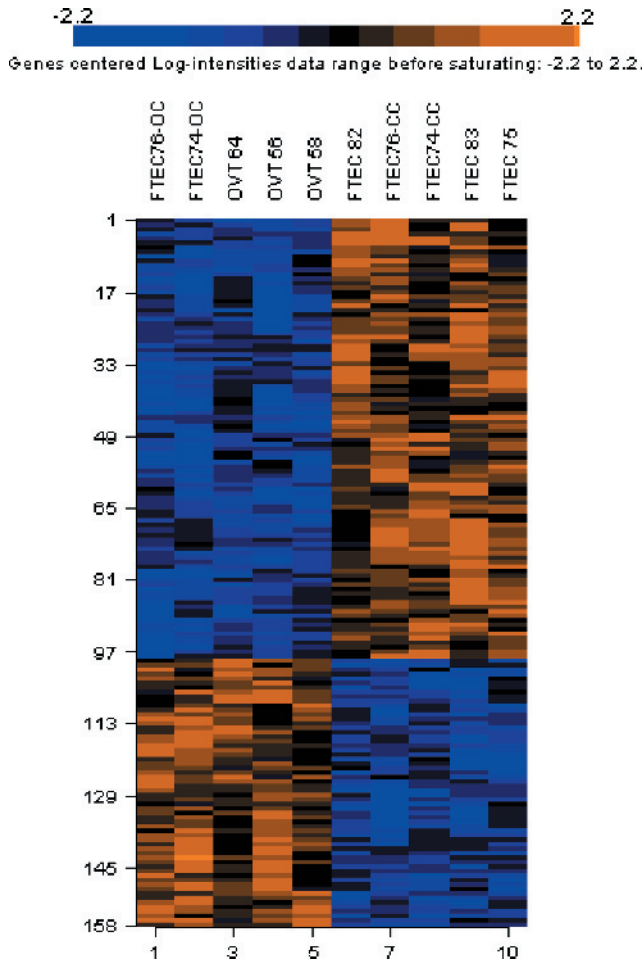| Laboratory Designation	Addgene No. or Other ID	Hyperlink
Viral cocktail		
A	shBRCA1-308*	*Homo sapiens* breast cancer 1, early onset (BRCA1) … — Nucleotide result
C	shBRCA1-4590[†]	*Homo sapiens* breast cancer 1, early onset (BRCA1) … — Nucleotide result
S	1774	Addgene — pBABE-neo-hTERT plasmid data
T	9058	Addgene — pBABE-hygro p53 DD plasmid data
EE	9051	Addgene — pBABE puro H-Ras V12 plasmid data
GG	11129	Addgene — pbabe-cyclin D1 + CDK4R24C plasmid data
MM	18773	Addgene — MSCV Myc T58A puro plasmid data
PP	13970	Addgene — pBABE-puro SV40 LT plasmid data
AA	10668	Addgene — pBABE GFP plasmid data
Control cocktail		
AA	10668	Addgene — pBABE GFP plasmid data
G	pMMP-mir-gl2shRNA	
Q	pBabe-puro (empty vector)	

*Sequence: 5′-TGCTGTTGACAGTGAGCG CCCACAAAGTGTGACCACATAT TAGTGAAGCCACAGATGTA ATATGTGGTCACACTTTGTGGA TGCCTACTGCCTCGGA.
[†]Sequence: 5′-TGCTGTTGACAGTGAGCG CGGAGCTGGACACCTACCTGAT TAGTGAAGCCACAGATGTA ATCAGGTAGGTGTCCAGCTCCT TGCCTACTGCCTCGGA.

Table W2. Antibody Information for Immunohistochemistry.

Target	Vendor	Catalog No.	Dilution
p53	Dako	M7001	1:10
Cytokeratin 7	Dako	M7018	1:800
Cytokeratin 20	Dako	M7019	1:100
WT1	Thermo Scientific	PA1-38864	1:2
PAX8	ProteinTech Group	10336-1-AP	1:200
HE4 (WFDC2)	Abcam	ab24480	1:40

Dako, Carpinteria, CA; ProteinTech, Chicago, IL; Abcam, Cambridge, MA.

Figure W1. Hierarchical clustering of malignant signature. A total of 158 genes differentiating FTEC-OC and primary serous ovarian cancers from FTEC-CC and untreated normal primary FTEC were identified using F test ($P < .005$) and subjected to hierarchical clustering. Expression levels of each gene are presented in Table W3.

Gene No.	ProbeSet	Symbol	Name	EntrezID
1	224519_at	LOC10013	hypothetica	100132167
2	201309_x_	C5orf13	chromoson	9315
3	239487_at	FAM98A	family with	25940
4	226997_at	ADAMTS1:	ADAM met	81792
5	205533_s	CDH6	cadherin 6,	1004
6	213248_at	LOC73010	hypothetica	730101
7	1564002_a	AKD1	adenylate k	221264
8	204345_at	COL16A1	collagen, ty	1307
9	224818_at	SORT1	sortilin 1	6272
10	204966_at	BAI2	brain-speci	576
11	218963_s	KRT23	keratin 23 (	25984
12	227236_at	TSPAN2	tetraspanin	10100
13	210943_s	LYST	lysosomal t	1130
14	219468_s	CUEDC1	CUE doma	404093
15	236254_at	VPS13B	vacuolar pr	157680
16	203159_at	GLS	glutaminas	2744
17	220580_at	BICC1	bicaudal C	80114
18	1557289_s	GTF2IRD2	GTF2I repe	84163
19	213349_at	TMCC1	transmemb	23023
20	209198_s	SYT11	synaptotag	23208
21	226550_at	NA	NA	NA
22	1556051_a	BICD1	bicaudal D	636
23	215785_s	CYFIP2	cytoplasmi	26999
24	211066_x_	NA	NA	NA
25	205717_x_	NA	NA	NA
26	209079_x_	NA	NA	NA
27	1553300_a	DGKH	diacylglyce	160851
28	1570393_a	EML5	echinoderm	161436
29	216869_at	PDE1C	phosphodie	5137
30	236344_at	PDE1C	phosphodie	5137
31	221950_at	EMX2	empty spira	2018

Figure W1. (*continued*).

#	Probe	Symbol	Description	ID
32	239218_at	NA	NA	NA
33	1555673_a	LOC73075	keratin ass	730755
34	202117_at	ARHGAP1	Rho GTPas	392
35	236129_at	GALNT5	UDP-N-ace	11227
36	235489_at	RHOJ	ras homolo	57381
37	243481_at	RHOJ	ras homolo	57381
38	209631_s	GPR37	G protein-c	2861
39	235369_at	C14orf28	chromoson	122525
40	1555575_a	KDELR1	KDEL (Lys	10945
41	46142_at	LMF1	lipase matu	64788
42	202952_s	ADAM12	ADAM met	8038
43	204797_s	EML1	echinoderm	2009
44	202439_s	IDS	iduronate 2	3423
45	215836_s	NA	NA	NA
46	211966_at	COL4A2	collagen, ty	1284
47	223095_at	MARVELD	MARVEL d	83742
48	228141_at	GPX8	glutathione	493869
49	223392_s	TSHZ3	teashirt zin	57616
50	242873_at	NA	NA	NA
51	225615_at	IFFO2	intermediat	126917
52	37408_at	MRC2	mannose re	9902
53	219582_at	OGFRL1	opioid grow	79627
54	239817_at	NA	NA	NA
55	201283_s	TRAK1	trafficking p	22906
56	229557_at	MEG3	maternally	55384
57	206806_at	DGKI	diacylglyce	9162
58	214803_at	NA	NA	NA
59	230669_at	RASA2	RAS p21 p	5922
60	228885_at	NA	NA	NA
61	202688_at	TNFSF10	tumor necr	8743
62	203662_s	TMOD1	tropomodu	7111
63	226069_at	PRICKLE1	prickle hom	144165
64	226065_at	PRICKLE1	prickle hom	144165
65	230708_at	PRICKLE1	prickle hom	144165
66	222020_s	NTM	neurotrimin	50863
67	227566_at	NTM	neurotrimin	50863
68	213273_at	ODZ4	odz, odd O	26011
69	231382_at	FGF18	fibroblast g	8817
70	206987_x	FGF18	fibroblast g	8817
71	211029_x	FGF18	fibroblast g	8817
72	222281_s	NA	NA	NA
73	232720_at	LINGO2	leucine rich	158038
74	227750_at	KALRN	kalirin, Rho	8997
75	202687_s	TNFSF10	tumor necr	8743
76	203895_at	PLCB4	phospholip	5332
77	203896_s	PLCB4	phospholip	5332
78	214329_x	TNFSF10	tumor necr	8743
79	203157_s	GLS	glutaminas	2744
80	228101_at	APBA1	amyloid be	320
81	225807_at	JUB	jub, ajuba h	84962
82	238827_at	NA	NA	NA
83	236038_at	NA	NA	NA
84	209453_at	SLC9A1	solute carri	6548
85	230119_at	NA	NA	NA
86	244708_at	FLJ33996	hypothetica	283401
87	236364_at	NA	NA	NA
88	1555028_a	BRD3	bromodom	8019
89	228728_at	C7orf58	chromoson	79974
90	219610_at	RGNEF	190 kDa gu	64283
91	227657_at	RNF150	ring finger p	57484
92	239582_at	PML	promyelocy	5371
93	1558622_a	ZNF548	zinc finger	147694
94	238417_at	PGM2L1	phosphoglu	283209
95	1598_g_at	GAS6	growth arre	2621
96	208712_at	CCND1	cyclin D1	595
97	210642_at	CCIN	calicin	881
98	243795_s	LOC44090	hypothetica	440900
99	206577_at	VIP	vasoactive	7432
100	234977_at	ZADH2	zinc binding	284273
101	1555167_s	NAMPT	nicotinamic	10135
102	210854_x	SLC6A8	solute carri	6535
103	1566518_a	NA	NA	NA
104	216857_at	NA	NA	NA
105	227757_at	CUL4A	cullin 4A	8451

Figure W1. (*continued*).

Figure W1. (*continued*).

|				
106	225942_at	NLN	neurolysin	57486
107	1564315_a	C8orf49	chromoson	606553
108	203036_s	MTSS1	metastasis	9788
109	212849_at	AXIN1	axin 1	8312
110	239042_at	TSR1	TSR1, 20S	55720
111	212434_at	GRPEL1	GrpE-like 1	80273
112	212656_at	TSFM	Ts translati	10102
113	216411_s	NA	NA	NA
114	1555804_a	YSK4	YSK4 Sps1	80122
115	210215_at	TFR2	transferrin	7036
116	207463_x	PRSS3	protease, s	5646
117	213421_x	PRSS3	protease, s	5646
118	225078_at	EMP2	epithelial m	2013
119	213226_at	CCNA2	cyclin A2	890
120	221957_at	PDK3	pyruvate de	5165
121	211561_x	MAPK14	mitogen-ac	1432
122	216014_s	NA	NA	NA
123	217973_at	DCXR	dicarbonyl/	51181
124	1553031_a	GPR115	G protein-c	221393
125	213449_at	POP1	processing	10940
126	207558_s	PITX2	paired-like	5308
127	225862_at	SLC25A26	solute carri	115286
128	236146_at	SYNCRIP	synaptotag	10492
129	206947_at	B3GALT5	UDP-Gal:b	10317
130	223292_s	MRPS15	mitochondr	64960
131	231182_at	WIPF1	WAS/WAS	7456
132	1569588_x	PIK3C2A	phosphoinc	5286
133	217558_at	CYP2C9	cytochrome	1559
134	241606_s	TRUB1	TruB pseud	142940
135	203759_at	ST3GAL4	ST3 beta-g	6484
136	231099_at	FKBP15	FK506 bind	23307
137	230825_at	NA	NA	NA
138	213309_at	PLCL2	phospholip	23228
139	1555553_a	SLC22A7	solute carri	10864
140	235412_at	ARHGEF7	Rho guanir	8874
141	205449_at	SAC3D1	SAC3 dom	29901
142	218443_s	DAZAP1	DAZ assoc	26528
143	243526_at	WDR86	WD repeat	349136
144	243033_at	TWF1	twinfilin, ac	5756
145	1556558_s	FLJ36665	hypothetica	285266
146	204798_at	MYB	v-myb mye	4602
147	214664_at	PAICS	phosphorib	10606
148	216298_at	NA	NA	NA
149	233670_at	NA	NA	NA
150	240863_at	CYP19A1	cytochrome	1588
151	229446_at	NA	NA	NA
152	214540_at	HIST1H2B	histone clu	8348
153	227925_at	FLJ39051	hypothetica	399972
154	1554314_a	C6orf141	chromoson	135398
155	1560460_a	NA	NA	NA
156	244523_at	MMD	monocyte t	23531
157	218590_at	C10orf2	chromoson	56652
158	220616_at	ZNF384	zinc finger	171017

Figure W1. (*continued*).
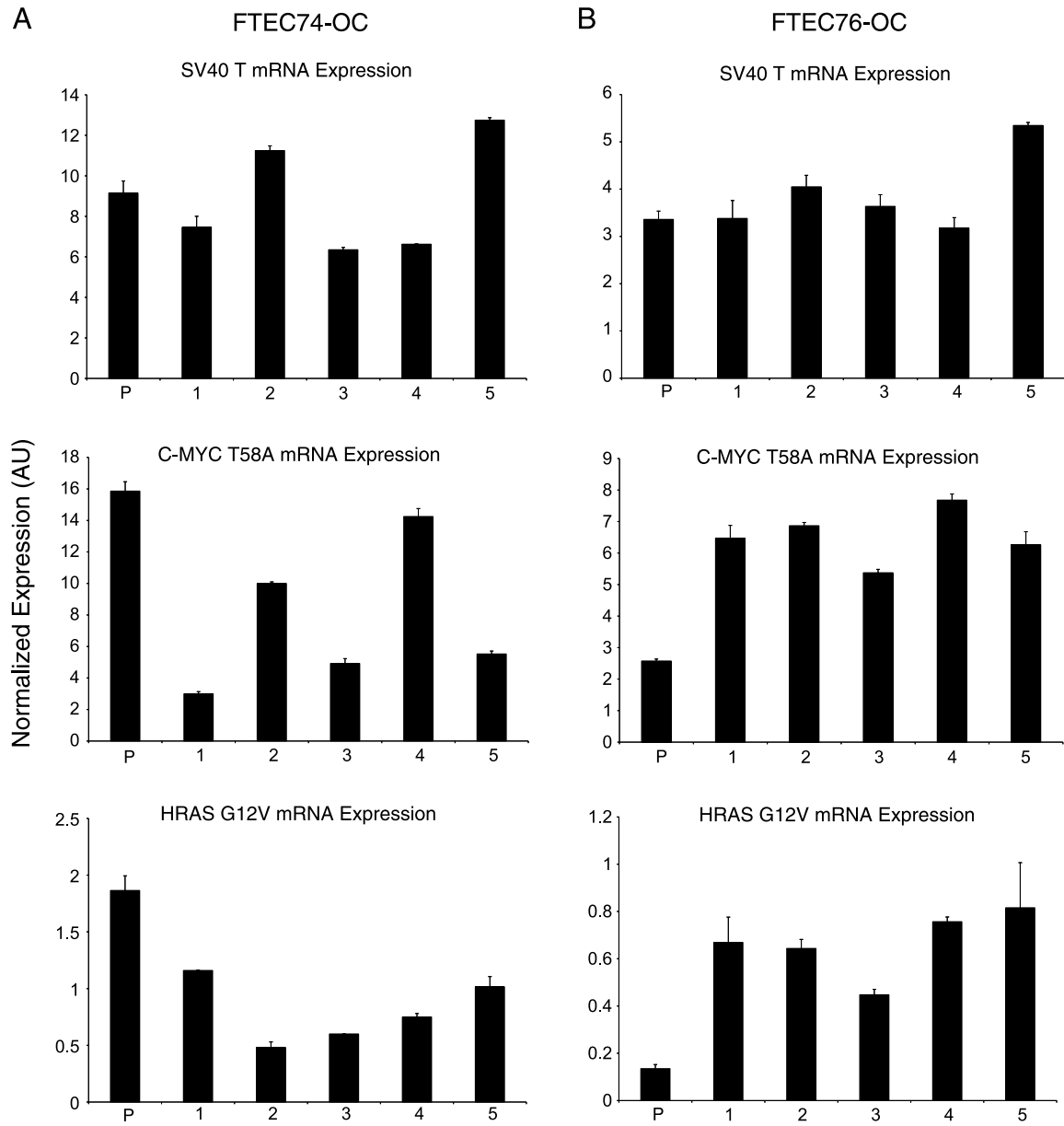
Figure W2. Clonal analysis of transformed FTEC lines. Expression levels of SV40 T, HRAS G12V, and C-MYC T58A in the parental (P) and five clonal sublines (numbered 1–5) of FTEC74-OC (A) and FTEC76-OC (B) using real-time RT-PCR. Error bars represent SD of replicates.